Exclusion limits on a scalar decaying to photons and distinguishing its production mechanisms

Tanumoy Mandal*

Department of Physics and Astronomy,
Uppsala University, Box 516, SE-751 20 Uppsala, Sweden

Abstract

LHC run-II has a great potential to search for new resonances in the diphoton channel. Latest 13 TeV data already put stringent limits on the cross sections in the diphoton channel assuming the resonance is produced through the gluon-gluon fusion. Many beyond the Standard Model (SM) theories predict TeV-scale scalars which copiously decay to diphotons. Apart from the gluon-gluon fusion production, these scalars can also be dominantly produced in other ways too at the LHC namely through the quark-quark fusion or the gauge boson fusions like the photon-photon, photon-Z, WW or ZZ fusions. In this paper, we use an effective field theory approach where a heavy scalar can produce in various ways and recast the latest CMS diphoton resonance search data to put model-independent limits on its mass and effective couplings to the SM particles. If a new scalar is discovered at the LHC, it would be very important to identify its production mechanism in order to probe the nature of the underlying theory. We show that combining various kinematic variables in a multivariate analysis can be very powerful to distinguish different production mechanisms one from the other.

arXiv:1612.01192v1 [hep-ph] 4 Dec 2016

* tanumoy.mandal@physics.uu.se

I. INTRODUCTION

There are numerous theoretical motivations to expect that the Standard Model (SM) is not the complete story and the scalar spectrum of the bigger theory may be richer than to possess only one neutral scalar - the Higgs boson. From this expectation, searches for new scalars are continuously being carried out at the Large Hadron Collider (LHC) in various channels. Along these directions, no confirm hint has been found so far in any of these searches. Nevertheless, some statistically significant results in some of these searches have drawn significant attention in the high energy physics community recently. Among them, the most famous one is the 750 GeV diphoton excess [1, 2] which created a lot of excitements in the community. Before the excess turned out to be a statistical fluke, numerous attempts have been made to explain the excess (see Ref. [3] for a review and a long list of references). Another important excess was the diboson excess around 2 TeV resonance mass [4–6] which also later turned out to be a statistical fluctuation.

Searches for heavy scalars at the LHC are generally being carried out in diphoton, diboson or dijet resonance searches. Diphoton channel, among them, is particularly important as this channel provides a comparatively cleaner background. Higgs was discovered first in the diphoton channel at the LHC [7, 8]. TeV-scale scalars decaying into diphoton system is one of the key predictions of many beyond the Standard Model (BSM) theories. Various possibilities have been extensively explored in context of the 750 GeV diphoton excess (see the reference list of [3] for various models that predict TeV-scale diphoton resonance). To test these predictions, LHC run-II provides us a great opportunity to observe a diphoton resonance of mass up to a few TeV. In this paper, we particularly focus on the diphoton final state for these reasons.

If a particle decays to diphotons, it must either be spin-0 or spin-2 in nature as the spin-1 particles decay to on-shell diphotons is forbidden by the Landau-Yang theorem [9, 10]. A spin-2 particle or graviton couples universally to all matter fields through energy-momentum tensor. Therefore, if a resonance in diphoton system mediated by graviton is observed, one would expect resonances at same mass in other possible channels also. Therefore, simultaneous studies in various channels might be more illuminating for the spin-2 particle. The current limits on the graviton mass is already quite high, around $\sim 2-3$ TeV. On the other hand, scalars of mass ~ 1 TeV decaying into diphotons, which is a typical signature of many models, still allowed by the LHC data. These scalars can be produced at the LHC in various ways *viz.* through the gg, qq, $\gamma\gamma$, γZ, WW or ZZ fusions. In this paper, we consider a (model-independent) effective field theory (EFT) approach where the scalar can be produced and decays (two-body) in different possible ways as mentioned. But, we only concentrate on the diphoton decay mode in this paper as stated earlier.

First, we derive the available parameter space for a scalar produced in different ways and decays to diphotons using our EFT approach. These limits will be grossly model-independent limits and can be used to set limits on other models wherever applicable. If a scalar resonance is actually be seen in future, the most obvious question that will arise is - how the scalar is produced? A most common way to decipher the production mechanism of a heavy scalar is to look at various kinematic distributions especially various jet observables which are important in this regard. This has been investigated to some extent in the literature in context of the 750 GeV diphoton excess [11–15]. In this paper, we revisit some of the jet observables and show their effectiveness in distinguishing different production modes. We, then, use a multivariate analysis (MVA) by combining

many kinematic variables to distinguish different production modes more efficiently.

This paper is organized as follows: in Section II, we employ an effective Lagrangian for a scalar ϕ, in Section III we discuss about the decays and various production modes of ϕ at the LHC and derive exclusion limits on the mass and couplings from the latest diphoton resonance search data. In the same section, we discuss how two different production modes of ϕ can be distinguished using a MVA analysis. Finally, we conclude in Section IV.

II. EFFECTIVE LAGRANGIAN

We consider an EFT approach where a scalar ϕ interacts with the SM gauge bosons through dimension-5 operators and with the SM quarks through dimension-4 operators. Assuming the scalar is a CP-even real scalar, we employ the following effective Lagrangian,

$$\begin{aligned}\mathcal{L} \supset & -\frac{\kappa_{gg}}{4\Lambda}\,\phi G^a_{\mu\nu}G^{a;\mu\nu} - \frac{\kappa_{\gamma\gamma}}{4\Lambda}\,\phi A_{\mu\nu}A^{\mu\nu} - \frac{\kappa_{ZZ}}{4\Lambda}\,\phi Z_{\mu\nu}Z^{\mu\nu} \\ & - \frac{\kappa_{\gamma Z}}{2\Lambda}\,\phi A_{\mu\nu}Z^{\mu\nu} - \frac{\kappa_{WW}}{2\Lambda}\,\phi (W^+)_{\mu\nu}(W^-)^{\mu\nu} - \sum_q \frac{\kappa_{qq}v}{\Lambda}\,\phi\bar{q}q\ . \end{aligned} \tag{1}$$

where the field-strength tensors corresponding to gluon (g), photon (γ), $W^\pm$ and Z bosons are $G^a_{\mu\nu}$, $A_{\mu\nu}$, $(W^\pm)_{\mu\nu}$ and $Z_{\mu\nu}$ respectively, and their generic form is, $\mathcal{V}_{\mu\nu} = \partial_\mu\mathcal{V}_\nu - \partial_\nu\mathcal{V}_\mu$ where $\mathcal{V} = \{g, \gamma, W^\pm, Z\}$. All the dimension-5 operators are suppressed by the new physics scale Λ. In general, Λ could be different for different operators, but we assume they are same for all the operators. Only the $\phi\bar{q}q$ is a dimension-4 operator and we introduce the electroweak symmetry breaking scale $v \approx 246$ GeV in association with κ_{qq} to bring the scale Λ in the interaction. The scalar ϕ can, in general, couple differently with different SM quarks. For simplicity, in this analysis, we assume a single coupling κ_{qq} same for all the SM quarks. We use the notation κ_{xy} to denote a generic dimensionless coupling associated with the operators. Note that in all interactions with gauge bosons, the normalization factor are so chosen such that the corresponding Feynman rule takes the form,

$$(i\kappa_{xy}/\Lambda)\left(g^{\alpha\beta}p_1\cdot p_2 - p_1^\beta p_2^\alpha\right)\ , \tag{2}$$

where p_1 and p_2 are the 4-momenta of two gauge bosons $\mathcal{V}^\alpha$ and $\mathcal{V}'^\beta$ respectively directed towards the vertex. The Feynman rule for the $\phi\bar{q}q$ interaction is $i\kappa_{qq}v/\Lambda$.

III. PHENOMENOLOGY

In addition to the SM Lagrangian, we implement the effective Lagrangian of ϕ shown in Eq. (1) in FeynRules [16] to generate the Universal FeynRules Output [17] model files for the MadGraph [18] event generator. We use the MMHT14LO [19] parton distribution functions (PDFs) for event generation. This PDF set includes the photon PDF which has been computed following the approach described in [12, 20]. We use factorization scale μ_F and renormalization scale μ_R at M_ϕ in our analysis. Generated events are further showered and hadronized including multiple parton interactions by using Pythia8 [21]. Detector simulation is performed by implementing CMS selection cuts [22] in Delphes [23] which uses the FastJet [24] package for jet clustering. We use

the anti-k_T algorithm [25] with $R = 0.4$ for jet clustering. For MVA, we use the Boosted Decision Tree (BDT) algorithm in the TMVA [26] framework.

A. Decays of ϕ

From the Lagrangian in Eq. (1), we have the following two-body decay modes of ϕ *viz.* $\phi \to xy$ where $xy = \{gg, qq, \gamma\gamma, \gamma Z, WW, ZZ\}$. The partial widths for these decay modes are given by the following expressions,

$$\Gamma_{gg} = \frac{\kappa_{gg}^2 M_\phi^3}{8\pi\Lambda^2}; \quad \Gamma_{qq} = \frac{3\kappa_{qq}^2 v^2 M_\phi}{8\pi\Lambda^2}\left(1 - \frac{M_q^2}{M_\phi^2}\right)^{\frac{3}{2}}; \quad \Gamma_{\gamma\gamma} = \frac{\kappa_{\gamma\gamma}^2 M_\phi^3}{64\pi\Lambda^2};$$
$$\Gamma_{\gamma Z} = \frac{\kappa_{\gamma Z}^2 M_\phi^3}{32\pi\Lambda^2}\left(1 - \frac{M_Z^2}{M_\phi^2}\right)^3; \quad \Gamma_{VV} = \frac{\kappa_{VV}^2 M_\phi^3}{32\pi\Lambda^2}\left(1 - \frac{M_V^2}{M_\phi^2}\right)^{\frac{1}{2}}\left(1 - \frac{4M_V^2}{M_\phi^2} + \frac{6M_V^4}{M_\phi^4}\right) , \quad (3)$$

where V denotes the electroweak gauge bosons W and Z. There could be subdominant three-body decays of ϕ possible mediated through an off-shell gauge boson. If the intermediate gauge boson is massless, in case of gluons or photon, the three-body branching ratios (BRs) are non-negligible especially when M_ϕ is large [27]. In this analysis, we consider the two-body and three-body decays of ϕ to obtain the total width where the three-body decay widths are computed numerically using MadGraph. Partial widths for three-body decay modes where an off-shell gauge boson goes to W^+W^- pair grow very rapidly with increasing scalar mass. This is due to the contribution coming from the longitudinal polarizations of W bosons. Therefore, in high mass region, BR for $\phi \to \gamma\gamma$ reduces substantially.

B. Production of ϕ at the LHC

When all κ_{xy} in Eq. 1 are nonzero, the scalar can produce at the LHC from the gg, qq, $\gamma\gamma$, γZ, WW and ZZ fusions. In Fig. 1, we show the partonic cross sections of various production modes of ϕ at the 13 TeV LHC for $\kappa_{xy} = 1$ and $\Lambda = 1$ TeV. Initial W and Z come from the initial quark splitting. Therefore, ϕ is produced in association with at least two jets for the $VV \to \phi$ type of productions. Similarly, for the γZ initiated production, ϕ is produced in association with at least one jet. Partonic cross sections are computed by applying the following generation level cuts on the jets wherever applicable

$$p_T(j) > 20 \text{ GeV}; \quad |\eta(j)| < 5; \quad \Delta R(jj) > 0.4 \, . \quad (4)$$

Note that all cross sections scale as $(\kappa_{xy}/\Lambda)^2$, and therefore, we present them by choosing $k_{xy} = 1$ and $\Lambda = 1$ TeV such that one can translate it easily for other values.

For all six types of production of ϕ, we generate parton level events with up to two jets in the final state. These events are passed to Pythia8 [21]for showering and hadronization. This process may introduce double counting between the matrix element partons and the parton showers. To generate inclusive signal events by avoiding any double counting, we use the MLM matching [28] technique to match the matrix element partons with

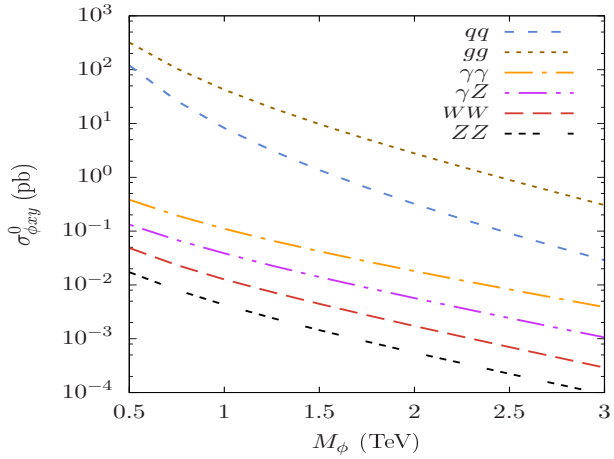

FIG. 1. Partonic cross sections of various production modes of ϕ as functions of M_ϕ computed at $\mu_R = \mu_F = M_\phi$ at the 13 TeV LHC. Here, $\sigma^0_{\phi xy}$ denotes the cross section of ϕ produced through the xy fusion with $\kappa_{xy} = 1$ and $\Lambda = 1$ TeV. Initial g, q and γ come from the PDFs of proton whereas initial W and Z come from initial quarks. These cross sections are computed by applying some basic generation level cuts (wherever applicable) as defined in Eq. (4).

the parton shower. Inclusive signal events including up to two jets for the gg, qq and $\gamma\gamma$ fusions are generated by combining the following processes,

$$\left.\begin{array}{lllll} pp & \to & (\phi) & \to & \widehat{\gamma\gamma}\,, \\ pp & \to & (\phi\; j) & \to & \widehat{\gamma\gamma}\; j\,, \\ pp & \to & (\phi\; jj) & \to & \widehat{\gamma\gamma}\; jj\,. \end{array}\right\} \tag{5}$$

where we set the matching scale $Q_{cut} \sim 125$ GeV. The curved connections above two photons signify that they come from the decay of ϕ. To determine the appropriate Q_{cut} for these production processes, we have done three important checks *viz.* smooth transition in the differential jet-rate distributions between events with N and $N+1$ jets, matched cross sections are within $\sim 10\%$ of the zero jet contribution and also not vary much with Q_{cut} variation once we have chosen it properly. For the γZ, WW or ZZ fusion productions, the initial W or Z come from the quark splitting and we have additional jets at the Born level process. Therefore, the WW and ZZ fusion events are generated only at the $pp \to \phi jj$ level and no matching is required for these cases. But for the γZ fusion we do use matching by combining the processes $\gamma p \to \phi j$ and $pp \to \phi jj$ with $Q_{cut} \sim 30$ GeV. The dominant (about 90% of the total) $\gamma\gamma$ background comes from the $q\bar{q} \to \gamma\gamma$ process. We generate this background by matching up to 2 jets with $Q_{cut} \sim 20$ GeV.

C. Exclusion from the LHC data

Diphoton resonance searches at the LHC using run-I and run-II data set strong upper limits (ULs) on $\sigma \times$ BR of a spin-0 or spin-2 resonances. It should be noted that these searches are generally optimized for an s-channel resonance production through the gg fusion decaying to two photons. Depending on the different production mechanisms of the resonance, the selection cut efficiencies can significantly vary. For a particular production

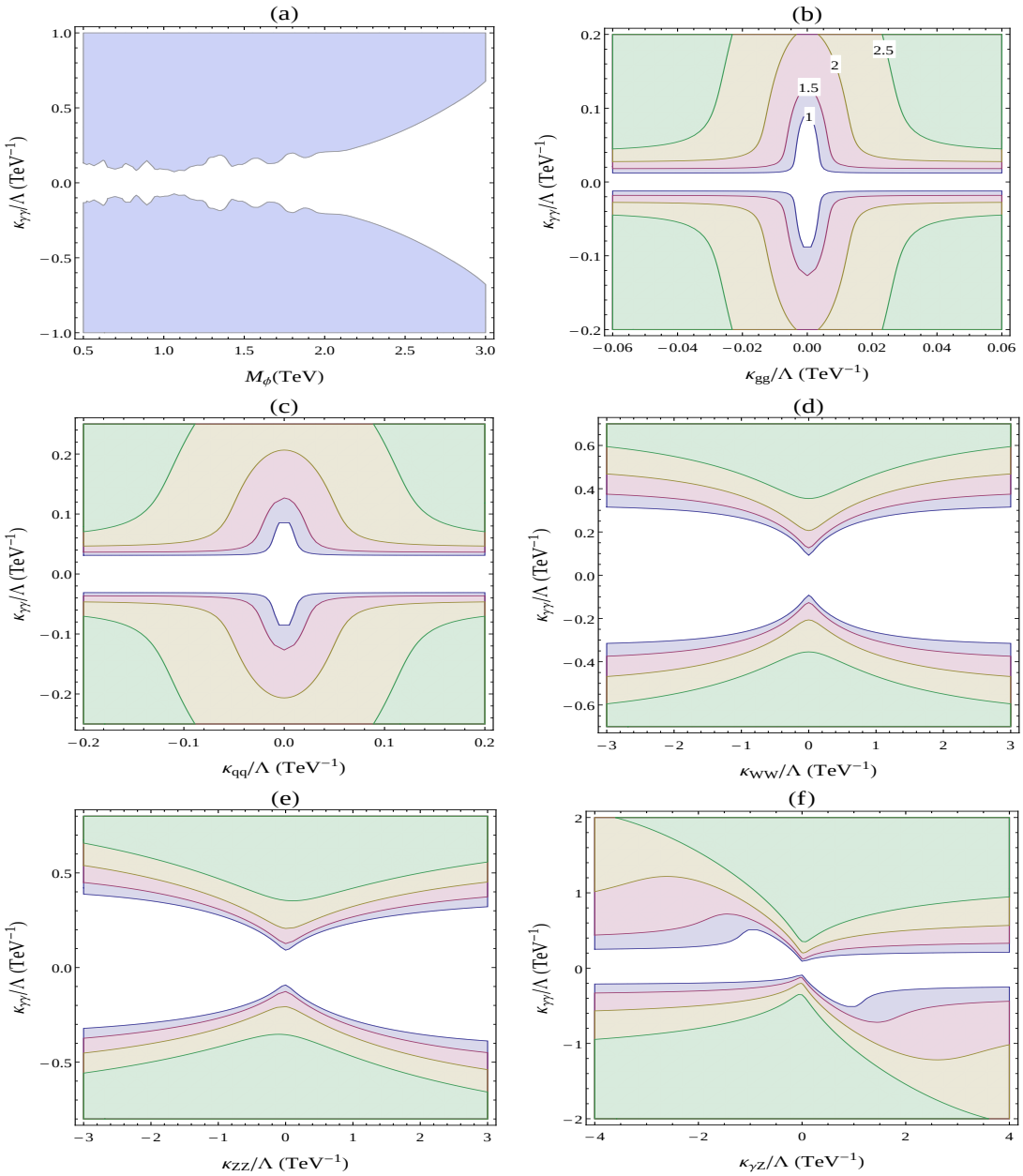

FIG. 2. Exclusion regions from the observed UL on cross sections for the CMS diphoton resonance search data at the 13 TeV (a) Exclusions in the $M_\phi - \kappa_{\gamma\gamma}/\Lambda$ plane setting all other $\kappa_{xy} = 0$. (b)-(f) Exclusions in the $\kappa_{xy}/\Lambda - \kappa_{\gamma\gamma}/\Lambda$ plane while setting all other κ's to zero. The contours correspond to $M_\phi = 1, 1.5, 2$ and 2.5 TeV from outer to inner direction.

mechanism, cut efficiencies can also change on the number of selected photons and jets. Therefore, in order to derive exclusion limits on the model parameters by recasting the limits on $\sigma \times$ BR from an experiment, one has to properly take care the selection cut efficiencies in the analysis. This can be properly taken care of by using the following relation:

$$\mathcal{N}_s = \sigma_s \times \epsilon_s \times \mathcal{L} = \left(\sum_i \sigma_i \times \epsilon_i \right) \times \mathcal{L} \ , \tag{6}$$

where $\mathcal{N}_s$ is the UL on the number of signal events which can be written as the product of the signal cross section σ_s (produced through a particular mechanism used in the analysis), the corresponding signal cut efficiency ϵ_s and the luminosity $\mathcal{L}$. When different types of production mechanisms contribute to any experiment, $\mathcal{N}_s$ can be expressed by the sum $(\sum_i \sigma_i \times \epsilon_i) \times \mathcal{L}$. Here, i runs over all the contributing production mechanisms. Cut efficiencies can be different for different production mechanisms and also for different resonance masses. We find that it can vary up to $\sim 25\%$ for different production modes and also for different masses. As expected, in high mass region, $M_\phi \gtrsim 1$ TeV, cut efficiencies become insensitive to the mass.

We roughly employ the selection cuts used by the CMS collaboration for their 13 TeV diphoton resonance search analysis as listed below [22].

1. Transverse momentum of the selected photons and jets satisfy $p_T(\gamma), p_T(j) > 25$ GeV with two hardest photons satisfying $p_T(\gamma_1), p_T(\gamma_2) > 75$ GeV.

2. Pseudorapidity of the selected photons satisfy $|\eta(\gamma)| < 2.5$ excluding the barrel-endcap region $1.44 < |\eta(\gamma)| < 1.57$ (and rejecting events with both photons are in the endcap region) and jets $|\eta(j)| < 4.5$.

3. Separation in the η-ϕ plane between any two photons or photon-jet pair satisfy $\Delta R(\gamma, \gamma), \Delta R(\gamma, j) > 0.4$.

4. Invariant mass of the two hardest photons satisfies $M(\gamma_1, \gamma_2) > 230$ GeV and $M(\gamma_1, \gamma_2) > 320$ GeV for events with at least one photon is in the endcap region.

In general, all κ_{xy} can be nonzero at the same time, but this will make the analysis very complicated. To set exclusion limits, we choose, in addition to nonzero $\kappa_{\gamma\gamma}$ (since we are only interested in the diphoton final state), only one κ_{xy} is nonzero while setting all others to zero. We show the exclusion regions (colored) in the $\kappa_{xy}/\Lambda - \kappa_{\gamma\gamma}/\Lambda$ plane for four benchmark masses, $M_\phi = 1, 1.5, 2$ and 2.5 TeV. Only in Fig. 2(a), we show the exclusion regions (colored) in the $M_\phi - \kappa_{\gamma\gamma}/\Lambda$ plane assuming all κ_{xy} are zero except $\kappa_{\gamma\gamma}$. To derive these limits, we recast the 95% confidence level (CL) UL on the $\sigma \times BR$ for the $\gamma\gamma$ spin-0 resonance search by the CMS collaboration at the 13 TeV with 16.2 fb^{-1} integrated luminosity ($\mathcal{L}$) [22]. CMS analysis is done for different width choices of the resonance. In particular, we use the limit that derived assuming the width of the resonance is 1.4% of its mass. If the width of a particle is very small compared to its mass one can safely use the narrow width approximation (NWA). In all our results, we use the NWA ignoring any interference effect between the signal and the background. To include the higher order effect, we use a constant next-to-leading order (NLO) K-factor of 2 for the gg fusion [29]. The NLO corrections of a heavy scalar produced from the $b\bar{b}$ fusion is computed in [30] where it is found that the NLO K-factor is close to 1 for heavier scalar masses. If the scalar is produced from the light quark fusions, one might expect slightly bigger K-factor. Here, we assume it to be 1 since it is not available in the literature. For the $\gamma\gamma$, γZ, WW and ZZ we assume it to be 1.3 [31]. The actual values of the K-factors can be slightly different from the constant values we have used but they have very little effect on the exclusion limits. The highest value of $\kappa_{\gamma\gamma}/\Lambda$ that is excluded is ~ 0.1 around $M_\phi \sim 1$ TeV. By choosing a value for $\kappa_{\gamma\gamma}$, one can translate this limit on Λ. Choosing $\kappa_{\gamma\gamma} = 1$ for $M_\phi \sim 1$ TeV, one finds that $\Lambda \lesssim 10$ TeV is excluded.

The basic shape of the exclusion regions in Figs. 2(b) and 2(c) are different from the ones in Figs. 2(d), 2(e) and 2(f). This is because the gg and the qq fusion productions

dominate over the $\gamma\gamma$ fusion mode for $\kappa_{xy} = 1$ as seen in Fig. 1. On the other hand, cross sections for the WW, ZZ and γZ fusion modes are smaller than the $\gamma\gamma$ mode for unity κ_{xy}. One should also notice that exclusion regions in Figs. 2(e) and 2(f) are asymmetric around $\kappa_{\gamma\gamma} = 0$ axis. This is due to the interference effect between the $\gamma\gamma$ and the ZZ or γZ production modes. On the other hand, no interference is possible between the $\gamma\gamma$ and the gg, qq or WW fusion modes. In general, when $\kappa_{\gamma\gamma}$ and another κ_{xy} are nonzero, the production cross section can be expressed as

$$\sigma\left(M_\phi, \kappa_{xy}, \kappa_{\gamma\gamma}, \Lambda\right) = \Lambda^{-2}\left\{\kappa_{xy}^2\sigma_{xy}^0(M_\phi) + \kappa_{\gamma\gamma}^2\sigma_{\gamma\gamma}^0(M_\phi) + \kappa_{xy}\kappa_{\gamma\gamma}\sigma_I^0(M_\phi)\right\} \ , \tag{7}$$

where the σ_I^0 is the interference contribution and σ^0's in the *r.h.s.* are computed for $\kappa_{xy} = 1$ and $\Lambda = 1$ TeV. These σ's as function of mass have been computed numerically by interpolating the cross sections in the mass range $M_\phi = 0.5 - 3$ TeV. The selection cut efficiencies in general depend on M_ϕ and κ_{xy}. Including cut efficiencies in Eq. (7) (omitting the functional dependence), we get

$$\sigma \times \epsilon = \Lambda^{-2}\left\{\kappa_{xy}^2\sigma_{xy}^0\epsilon_{xy} + \kappa_{\gamma\gamma}^2\sigma_{\gamma\gamma}^0\epsilon_{\gamma\gamma} + \kappa_{xy}\kappa_{\gamma\gamma}\sigma_I^0\epsilon_I\right\} \ , \tag{8}$$

where ϵ_{xy} and $\epsilon_{\gamma\gamma}$ are the cut efficiencies for the pure xy and the $\gamma\gamma$ fusion production respectively and they are functions of M_ϕ only. But ϵ_I associated with the interference term is a function of M_ϕ, κ_{xy} and $\kappa_{\gamma\gamma}$. We have seen that ϵ_I is mostly sensitive to M_ϕ but not to the couplings. Therefore, for simplicity we use $\epsilon_I = \epsilon_{xy}(M_\phi)$ for $\kappa_{xy}^2\sigma_{xy}^0 > \kappa_{\gamma\gamma}^2\sigma_{\gamma\gamma}^0$ and $\epsilon_I = \epsilon_{\gamma\gamma}(M_\phi)$ for $\kappa_{\gamma\gamma}^2\sigma_{\gamma\gamma}^0 > \kappa_{xy}^2\sigma_{xy}^0$. Branching fraction in the $\gamma\gamma$ channel can be expressed as

$$BR_{\gamma\gamma}\left(M_\phi, \kappa_{xy}, \kappa_{\gamma\gamma}\right) = \frac{\kappa_{\gamma\gamma}^2\Gamma_{\gamma\gamma}(M_\phi)}{\kappa_{\gamma\gamma}^2\Gamma_{\gamma\gamma}(M_\phi) + \kappa_{xy}^2\Gamma_{xy}(M_\phi)} \ , \tag{9}$$

where Γ's are known analytically from Eq. 3. We derive the exclusion regions by using Eqs. (8) and (9) in Eq. (6).

D. Distinguishing different production modes

A way to distinguish different production modes of a heavy scalar is to look at various kinematic distributions especially the jet activities associated with the scalar. It was pointed out in Refs. [11–15] that the jet multiplicity (N_{jet}) distribution could be very important in this regard. In Fig. 3, we show the normalized N_{jet} distributions of various production modes of the scalar. These distributions are drawn assuming $M_\phi = 1$ TeV at the 13 TeV LHC with 50 fb^{-1} integrated luminosity. In order to effectively suppress the SM background, we select events by applying a cut on the diphoton invariant mass $|M_{\gamma\gamma} - M_\phi| < 150$ GeV in addition to the set of cuts defined earlier. We also show the N_{jet} distribution of the dominant SM diphoton background in both plots for comparison. The dominant background contribution of about 90% comes from the $q\bar{q} \to \gamma\gamma$ process and, in this analysis, we only consider this as the SM background. The error bars associated with the background consist of both statistical and systematic uncertainties. In Ref. [22], various components of the systematic uncertainty is discussed in detail. Systematic uncertainty is expected to be small when background distributions are obtained from data. For a conservative estimate, we consider a constant 20% systematic uncertainty in each bin. Total uncertainty is, then, obtained by adding statistical and systematic uncertainties in quadrature.

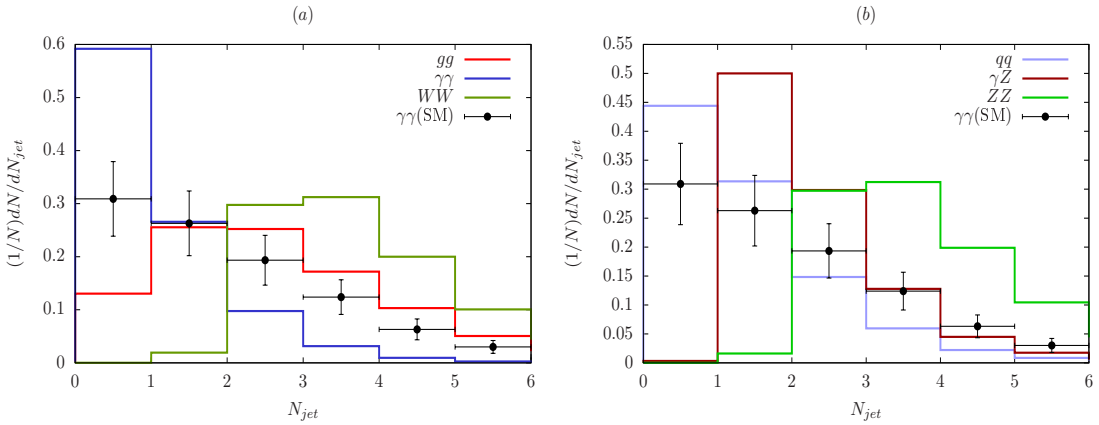

FIG. 3. Jet multiplicity (N_{jet}) distributions of various production modes of the scalar ϕ for $M_\phi = 1$ TeV at 13 TeV LHC. The N_{jet} distribution for the dominant SM background *i.e.* $pp \to \gamma\gamma$ process is shown on both plots with uncertainty which includes both the statistical and systematic parts. Statistical uncertainty is computed for $\mathcal{L} = 50$ fb^{-1} whereas we consider a constant 20% systematic uncertainty in each bin. The error bars represent the total uncertainty obtained adding statistical and systematic uncertainties in quadrature.

$gg \to \phi$	$qq \to \phi$	$\gamma\gamma \to \phi$	$\gamma Z \to \phi$	$WW \to \phi$	$ZZ \to \phi$	$\gamma\gamma$ SM
1.94	0.92	0.61	1.75	2.85	2.87	1.42

TABLE I. Average jet multiplicity for different production modes of ϕ at the 13 TeV LHC with $\mathcal{L} = 50$ fb^{-1}. Average jet multiplicity is defined by the sum, $\sum_i (BH)_i N_i$ where BH_i represents the bin height of the i-th bin of the normalized N_{jet} distribution and $N_i = i - 1$ is the number of jets associated with the i-th bin.

It is visibly clear that the different production modes display very different jet multiplicity distributions. The distributions for the $\gamma\gamma$ and the qq fusion modes peak at 0-jet but the peak for the qq mode not as sharp as the $\gamma\gamma$ one. The gg fusion shows a peak at 1 and 2-jet whereas the VBF production through the WW and ZZ fusions show peak at 2 and 3-jet. On the other hand, the γZ fusion mode shows a peak at 1-jet. Cross section for the 0-jet bin for the $\gamma\gamma$ mode is roughly about 60% of the total cross section. On the other hand, it is about 45% for the qq fusion case. The SM background N_{jet} distribution peaks at 0-jet, but contains only 30% of the total cross section. This nature can be quantized by the average jet multiplicity as shown in Table I. It is expected that if the scalar is produced through the $\gamma\gamma$ fusion, then the average jet multiplicity is lower compared to the gg or the qq fusions. On the other hand, the average jet multiplicity is higher for the VBF through the WW and ZZ modes compared to the gg or the qq fusions. For the $\gamma\gamma$ fusion, a hard jet in the final state can originate from the $q \to q\gamma$ splitting. However, this is suppressed compared to the leading order (LO) process with zero jet by the small probability of $q \to q\gamma$ branching and also by the smallness of α. On the other hand, colored particles in the initial state, *i.e.* in case of the gg or the qq fusions, lead to higher jet multiplicity compared to the $\gamma\gamma$ fusion. It is also well known that the jet multiplicity associated with the gg fusion is higher compared to the qq fusion. For the WW and ZZ fusion cases, one would generally anticipate at least two hard jets at the LO process since two initial V's come from the $q \to q'V$ branching. For the γZ

initial state, one expects at least one hard jet from the $q \to qZ$ splitting. Therefore, the jet multiplicity distribution peaks at 1-jet for the γZ fusion.

Mode:	$gg \to \phi$	$qq \to \phi$	$\gamma\gamma \to \phi$	$\gamma Z \to \phi$	$WW \to \phi$	$ZZ \to \phi$
$S \gg B$	3.6	3.4	8.9	10.0	30.4	30.3
$S = B$	0.9	0.8	2.2	2.5	7.6	7.6

TABLE II. The χ^2/dof values for the different production modes for two cases *viz.* $S \gg B$ and $S = B$. These are computed by considering up to $N_{jet} = 4$ for $M_\phi = 1$ TeV at the 13 TeV LHC with $\mathcal{L} = 50$ fb^{-1}.

One can define a χ^2 function to determine how much the observed data is compatible with the expected background. We define the following χ^2 function

$$\chi^2 = \sum_{i=1}^{N} \left(\frac{N_i^{obs} - N_i^{th}}{\Delta N} \right)^2 , \tag{10}$$

where the summation runs over the bins *e.g.* for the N_{jet} distribution $i = 1$ stands for 0-jet bin. Number of observed events is denoted by N_i^{obs} and N_i^{th} represents the number of expected events from the SM. The uncertainty ΔN is the total uncertainty which contains both the statistical and the systematic parts. If we assume the background (B) is much smaller than the signal (S), the obtained χ^2 per degrees of freedom (dof) for various production modes are shown in Table II. These are computed for 50 fb^{-1} integrated luminosity and for up to four jets. The number of dof then becomes $N_{dof} = 5-1 = 4$. One can see from Table II that χ^2/dof differs for different production mechanisms. Depending on these values, one can broadly categorize them into three categories. The gg and the qq production modes are more closer to the background compared to the $\gamma\gamma$ and the γZ modes. On the other hand, the expected background N_{jet} distribution drastically differ if the scalar is produced through the WW or the ZZ fusions. In reality, we always have some amount of background contamination in the signal. For $S/B = 1$, values of χ^2/dof still reasonably different for the different production modes as shown in Table II. Therefore, even in the presence of 50% background, one might still get some idea about the nature of the observed data by just computing χ^2/dof. One should remember that the jet activities might differ for different M_ϕ choices and also for the different center of mass energies ($\sqrt{S}$) of the colliding protons. These numbers are, therefore, for demonstration purpose but differ only qualitatively but not qualitatively for other sets of parameters.

E. Multivariate analysis

In the previous subsection, we show that the jet multiplicity distributions of two different production modes can be quite different. Using N_{jet} distribution as an example, we demonstrate that one can define a χ^2 function which can potentially act as a measure to distinguish two different production modes. Apart from the N_{jet} distribution, there are other kinematic variables which also show some differences in their shapes for different production modes. For example, in Ref. [11], the authors showed that various distributions like the scalar sum of transverse energy H_T, pseudorapidity (η) of the selected photons and jets, central rapidity gap ($\Delta\eta$) between the jets and the scalar show some visible differences for the gg and the $\gamma\gamma$ production modes.

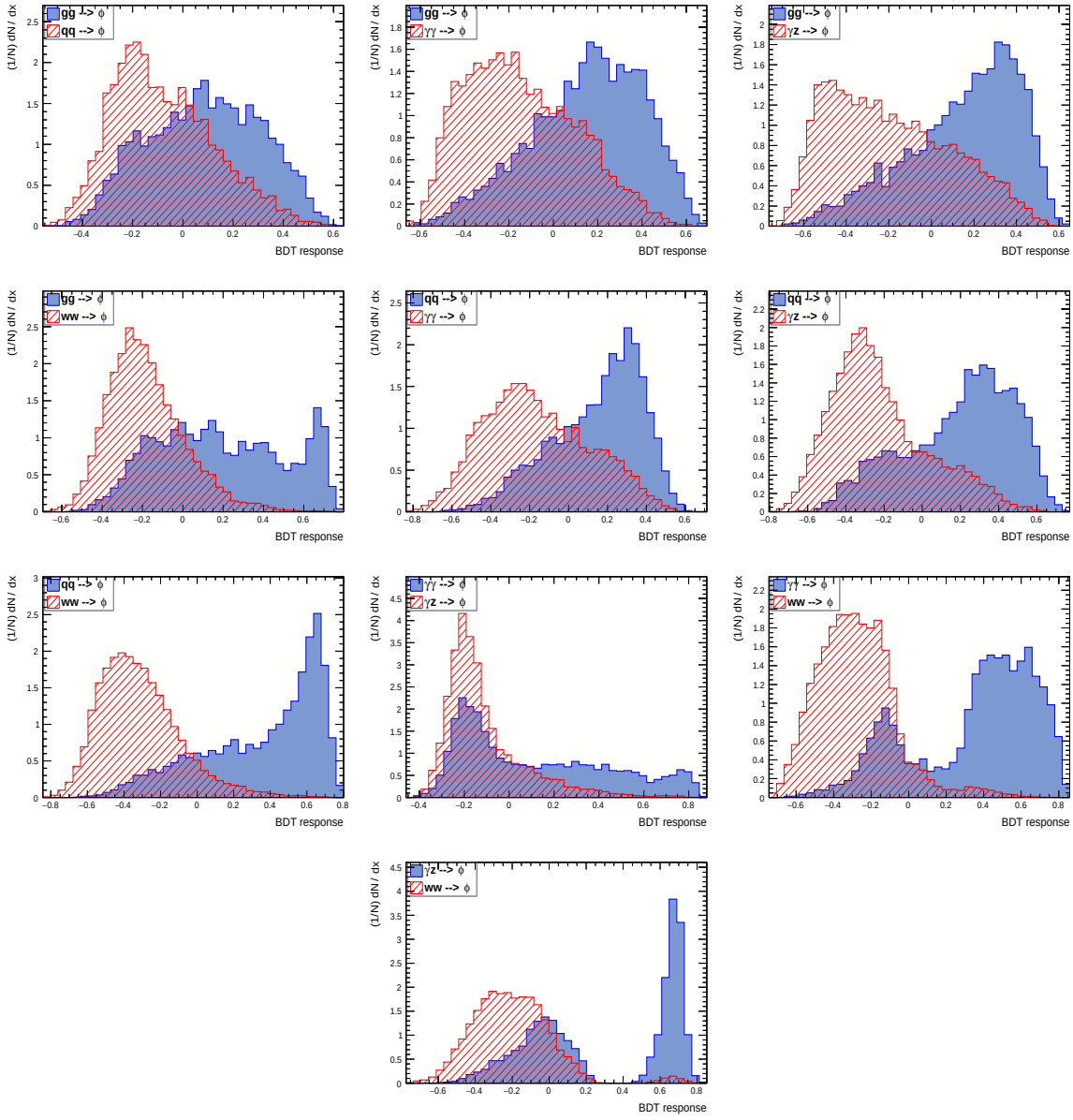

FIG. 4. BDT responses of two different production modes at a time. These are obtained using a MVA with twelve input variables as listed in Table III for $M_\phi = 1$ TeV at the 13 TeV LHC. Diphoton events are selected by applying $|M_{\gamma\gamma} - M_\phi| < 150$ GeV cut in addition to the CMS selection cuts as listed in the text.

Variable	Importance	Variable	Importance	Variable	Importance	Variable	Importance
N_{jet}	1.77×10^{-1}	$p_T(\gamma_1)$	4.87×10^{-2}	$\eta(\gamma_1)$	7.50×10^{-2}	$\Delta R(\gamma_1, \gamma_2)$	6.68×10^{-2}
H_T	4.48×10^{-2}	$p_T(\gamma_2)$	5.98×10^{-2}	$\eta(\gamma_2)$	6.21×10^{-2}	$\Delta R(\gamma_1, j_1)$	9.94×10^{-2}
$\Delta\eta(\phi, j_1)$	8.11×10^{-2}	$p_T(j_1)$	9.14×10^{-2}	$\eta(j_1)$	9.40×10^{-2}	$\Delta R(\gamma_2, j_1)$	1.00×10^{-1}

TABLE III. Input variables used for MVA to separate gg and $\gamma\gamma$ production modes and their relative importance.

In a similar spirit of χ^2, one can use many such kinematic variables for two different production modes that show some (small) differences in their shapes simultaneously in a multivariate analysis (MVA) whose output might show large differences in their shapes. Generally, MVA techniques are used to separate signal from background. Here, we use a MVA technique to distinguish two different production mechanisms more efficiently than a simple cut-based analysis or χ^2 analysis. We select events with at least one jet and construct twelve simple kinematic variables as shown in Table III for the MVA. This includes N_{jet}, H_T, $\Delta\eta$ between ϕ and leading jet, η and p_T of two selected photons and the leading jet and the separation ΔR in the $\eta - \phi$ plane between the photons and the leading jet. As an example, we show the gg and the $\gamma\gamma$ production modes and compute the relative importance of those variables in the BDT response. Greater relative importance of a variable signifies that variable is a better discriminator. From Table III, we see that N_{jet} is the best discriminator to differentiate the gg and the $\gamma\gamma$ production modes. Other variables like $\Delta R(\gamma_1, j_1)$, $\Delta R(\gamma_2, j_1)$, $p_T(j_1)$, $\eta(j_1)$ and $\Delta\eta(\phi, j_1)$ also act as good discriminators. It should be remembered that relative importance might change for other production modes and also for different parameters like M_ϕ, $\sqrt{S}$ etc. which can change the shapes of the kinematic distributions. It is important to mention that this set of twelve variables used here may not be the optimal one. One can always improve the analysis with cleverer choices of variables.

In Fig. 4, we show the BDT response when comparing two different production modes. The WW and the ZZ fusion modes are very similar in nature and therefore, it is extremely difficult to distinguish them. We show, by picking two production modes at a time, ten such possible BDT responses in Fig. 4 (we do not consider the ZZ fusion as it is very much identical to the WW mode). These responses are substantially different for most of the combinations and therefore can be distinguished very efficiently. We observe that it is hard to distinguish the $\gamma\gamma$ and the γZ production modes as their BDT responses are not very different from each other. One should notice that there are two peaks in the BDT responses of the WW mode. This is because two types of different topologies *i.e.* associated production and vector boson fusion contribute to the ϕjj final state.

As a side remark, one should always be very careful about overtraining for any MVA. This can happen without the proper choices of the algorithm specific tuning parameters. One can check whether a test sample is overtrained or not by using the Kolmogorov-Smirnov (KS) statistics. Generally, if KS probability lies within the range 0.1 to 0.9 guarantees that the test sample is not overtrained. For this purpose, one uses two statistically independent samples, one for training and the other for testing.

IV. CONCLUSIONS

Among the various resonance search channels at the LHC, the diphoton channels are particularly important as this channel provides a comparatively cleaner background. Generally, the diphoton resonance searches at the LHC assume that the resonance produces from the gg fusion. Apart from the gg fusion production, many BSM theories predict TeV-scale scalars that decay to diphotons can dominantly be produced by other means namely through the quark-quark (qq) fusion or through the gauge boson fusions ($\gamma\gamma$, γZ, WW and ZZ). In this paper, we consider an effective field theory of a heavy scalar that decays to diphotons. In this model independent approach, the scalar can be produced in all the possible types mentioned above. We derive exclusion limits on the mass and the

effective couplings of the scalar using the latest 13 TeV CMS diphoton resonance search data with $\mathcal{L} = 16.2$ fb^{-1}. While deriving the limits, we consider, for simplicity, only one effective coupling other than the $\kappa_{\gamma\gamma}$ (since we only focus on the diphoton final state) is nonzero. Selection cut efficiencies can change significantly for different production mechanisms. We have properly taken care of the modified cut efficiencies while recasting limits set by the CMS collaboration. We find that when the scalar dominantly produced from the $\gamma\gamma$ fusion, the latest LHC diphoton resonance search data sets limit on the new physics scale $\Lambda \gtrsim 10$ TeV for the coupling $\kappa_{\gamma\gamma} \sim 1$.

In future, if a scalar resonance is seen at the LHC in the diphoton channel, the immediate important issue one has to investigate that how the scalar is produced. Some preliminary analyses have already been done in context of the 750 GeV resonance where it is shown that the jet multiplicity distributions can be very different for the different production modes. In this paper, we revisit the issue and show that the average jet multiplicity and the N_{jet} distribution can act as good discriminators. For better discrimination, we use a sophisticated multivariate analysis by combining twelve simple kinematic variables to distinguish one production mechanism from the other. Our analysis shows that one can identify different production mechanisms very efficiently at the LHC.

ACKNOWLEDGMENTS

The author thank Valery A. Khoze, Lucian A. Harland-Lang, Rikard Enberg and Gunnar Ingelman for helpful discussions. This work is supported by the Swedish Research Council under contracts 621-2011-5107 and 2015-04814 and by the Carl Trygger Foundation under contract CTS-14:206.

---

[1] Morad Aaboud et al. Search for resonances in diphoton events at $\sqrt{s}$=13 TeV with the ATLAS detector. 2016.

[2] Vardan Khachatryan et al. Search for resonant production of high-mass photon pairs in proton-proton collisions at sqrt(s) = 8 and 13 TeV. 2016.

[3] Alessandro Strumia. Interpreting the 750 GeV digamma excess: a review. 2016.

[4] Georges Aad et al. Search for high-mass diboson resonances with boson-tagged jets in proton-proton collisions at $\sqrt{s} = 8$ TeV with the ATLAS detector. *JHEP*, 12:055, 2015.

[5] Georges Aad et al. Search for resonant diboson production in the $\ell\ell q\bar{q}$ final state in pp collisions at $\sqrt{s} = 8$ TeV with the ATLAS detector. *Eur. Phys. J.*, C75:69, 2015.

[6] Georges Aad et al. Search for production of WW/WZ resonances decaying to a lepton, neutrino and jets in pp collisions at $\sqrt{s} = 8$ TeV with the ATLAS detector. *Eur. Phys. J.*, C75(5):209, 2015. [Erratum: Eur. Phys. J.C75,370(2015)].

[7] Georges Aad et al. Observation of a new particle in the search for the Standard Model Higgs boson with the ATLAS detector at the LHC. *Phys. Lett.*, B716:1–29, 2012.

[8] Serguei Chatrchyan et al. Observation of a new boson at a mass of 125 GeV with the CMS experiment at the LHC. *Phys. Lett.*, B716:30–61, 2012.

[9] L. D. Landau. On the angular momentum of a system of two photons. *Dokl. Akad. Nauk Ser. Fizika,60,207-209*, 60:207–209, 1948.

[10] Chen-Ning Yang. Selection Rules for the Dematerialization of a Particle Into Two Photons. *Phys. Rev.*, 77:242–245, 1950.

[11] Csaba Cski, Jay Hubisz, Salvator Lombardo, and John Terning. Gluon versus photon production of a 750 GeV diphoton resonance. *Phys. Rev.*, D93(9):095020, 2016.

[12] L. A. Harland-Lang, V. A. Khoze, and M. G. Ryskin. The production of a diphoton resonance via photon-photon fusion. *JHEP*, 03:182, 2016.

[13] Markus A. Ebert, Stefan Liebler, Ian Moult, Iain W. Stewart, Frank J. Tackmann, Kerstin Tackmann, and Lisa Zeune. Exploiting jet binning to identify the initial state of high-mass resonances. *Phys. Rev.*, D94(5):051901, 2016.

[14] Mykhailo Dalchenko, Bhaskar Dutta, Yu Gao, Tathagata Ghosh, and Teruki Kamon. Exploring the Jet Multiplicity in the 750 GeV Diphoton Excess. *Phys. Lett.*, B761:77–80, 2016.

[15] Benjamin Fuks, Dong Woo Kang, Seong Chan Park, and Min-Seok Seo. Investigating the jet activity accompanying the production at the LHC of a massive scalar particle decaying into photons. *Phys. Lett.*, B761:344–349, 2016.

[16] Adam Alloul, Neil D. Christensen, Céline Degrande, Claude Duhr, and Benjamin Fuks. FeynRules 2.0 - A complete toolbox for tree-level phenomenology. *Comput. Phys. Commun.*, 185:2250–2300, 2014.

[17] Celine Degrande, Claude Duhr, Benjamin Fuks, David Grellscheid, Olivier Mattelaer, and Thomas Reiter. UFO - The Universal FeynRules Output. *Comput. Phys. Commun.*, 183:1201–1214, 2012.

[18] J. Alwall, R. Frederix, S. Frixione, V. Hirschi, F. Maltoni, O. Mattelaer, H. S. Shao, T. Stelzer, P. Torrielli, and M. Zaro. The automated computation of tree-level and next-to-leading order differential cross sections, and their matching to parton shower simulations. *JHEP*, 07:079, 2014.

[19] L. A. Harland-Lang, A. D. Martin, P. Motylinski, and R. S. Thorne. Parton distributions in the LHC era: MMHT 2014 PDFs. *Eur. Phys. J.*, C75(5):204, 2015.

[20] L. A. Harland-Lang, V. A. Khoze, and M. G. Ryskin. The photon PDF in events with rapidity gaps. *Eur. Phys. J.*, C76(5):255, 2016.

[21] Torbjorn Sjostrand, Stephen Mrenna, and Peter Z. Skands. A Brief Introduction to PYTHIA 8.1. *Comput. Phys. Commun.*, 178:852–867, 2008.

[22] Vardan Khachatryan et al. Search for high-mass diphoton resonances in proton-proton collisions at 13 TeV and combination with 8 TeV search. 2016.

[23] J. de Favereau, C. Delaere, P. Demin, A. Giammanco, V. Lematre, A. Mertens, and M. Selvaggi. DELPHES 3, A modular framework for fast simulation of a generic collider experiment. *JHEP*, 02:057, 2014.

[24] Matteo Cacciari, Gavin P. Salam, and Gregory Soyez. FastJet User Manual. *Eur. Phys. J.*, C72:1896, 2012.

[25] Matteo Cacciari, Gavin P. Salam, and Gregory Soyez. The Anti-k(t) jet clustering algorithm. *JHEP*, 04:063, 2008.

[26] Andreas Hocker et al. TMVA - Toolkit for Multivariate Data Analysis. *PoS*, ACAT:040, 2007.

[27] Ulf Danielsson, Rikard Enberg, Gunnar Ingelman, and Tanumoy Mandal. Heavy photophilic scalar at the LHC from a varying electromagnetic coupling. 2016.

[28] Michelangelo L. Mangano, Mauro Moretti, Fulvio Piccinini, and Michele Treccani. Matching matrix elements and shower evolution for top-quark production in hadronic collisions.

JHEP, 01:013, 2007.

[29] D. de Florian et al. Handbook of LHC Higgs Cross Sections: 4. Deciphering the Nature of the Higgs Sector. 2016.

[30] Csaba Balazs, Hong-Jian He, and C. P. Yuan. QCD corrections to scalar production via heavy quark fusion at hadron colliders. *Phys. Rev.*, D60:114001, 1999.

[31] K. Arnold et al. VBFNLO: A Parton level Monte Carlo for processes with electroweak bosons. *Comput. Phys. Commun.*, 180:1661–1670, 2009.